The Antares neutrino telescope : performance studies and analysis of first data

Bruijn, R.

Publication date
2008

Chapter 5

Detector performance

The performance of the full 12 line detector in the presence of background from atmospheric muons and random noise has been evaluated. For this purpose, the track reconstruction algorithm developed in this work is used. Neutrinos are considered as the exclusive source of upward going muons. Atmospheric muons thus only pose a background when the track reconstruction wrongly identifies these events as upward going. As these tracks are wrongly reconstructed, this should be reflected in quantities correlated to the quality of the fit. Cosmic neutrinos are only distinguishable from atmospheric neutrinos by their energy (harder spectrum for cosmic) or by association of their direction with a cosmic source. The aim is thus to reduce the background from atmospheric muons and random noise to below the level of the atmospheric neutrinos. The influence of the rate of random background is studied in detail.

In chapter 4, an analysis of the data from the first Antares detector line was presented. In that analysis, the result from a χ^2 minimization procedure was used. This requires the minimum amount of knowledge of the detection medium and apparatus, as it assumes the light to be emitted at the Cherenkov angle. For the analysis presented in this chapter, a likelihood fit is applied after the χ^2 minimization (see chapter 3).

This chapter starts with an introduction to the Monte Carlo simulation. Several quantities are identified which can be used to reduce the background. Finally, the efficiency and accuracy of the detector are evaluated after applying various cuts.

5.1 Monte Carlo

The simulated data samples used in this study are generated as described in chapter 2. Three separate data-sets are used. These are upward going neutrinos, downward going atmospheric muons and events from random background. These sets were generated for three levels of random background, those being

Rate	60 kHz	120 kHz	240 kHz
Livetime	173015.70 s	144179.75 s	86507.85 s
Triggered	3	4041	1526612
Reconstructed	1	623	187817
$\cos(\theta) > 0$	0	266	84561

Table 5.1: *Sample of simulated random background events used in this study.*

Rate	60 kHz		120 kHz		240 kHz	
Type	ν_μ	$\bar{\nu}_\mu$	ν_μ	$\bar{\nu}_\mu$	ν_μ	$\bar{\nu}_\mu$
Generated	$13 \cdot 10^{10}$	$13 \cdot 10^{10}$	$13 \cdot 10^{10}$	$13 \cdot 10^{10}$	$13 \cdot 10^{10}$	$13 \cdot 10^{10}$
$N_{photons} \geq 10$	255340	269587	255238	269270	255340	269373
Triggered	150544	156916	151082	157602	203498	214318
Reconstructed	145125	151243	135515	140660	134185	139501

Table 5.2: *Sample of simulated neutrino events used in this study.*

60 kHz, 120 kHz and 240 kHz per photo-multiplier tube. The grid size used in the reconstruction of the events at 60 and 120 kHz is set to 5 degrees. This is the same as in chapter 3. For the events with a background of 240 kHz, this grid size would lead to a prohibitively long time needed for the reconstruction with respect to the data-taking. Therefore the grid size is set to 10 degrees. Also for 240 kHz, the maximum transverse distance between two hits is reduced from 90 to 75 meters, which increases the purity of the hits. The characteristics of the samples are listed in tables 5.1, 5.2 and 5.3. In these tables, the label 'Rate' corresponds to the random background rate. In table 5.1, the label 'Livetime' corresponds to the effective livetime of the sample. The label 'Generated' corresponds to the total number of events generated and the label '$N_{photons} \geq 10$' corresponds to the number of events causing 10 or more detected photons. The numbers of triggered and reconstructed events are given in the rows with label 'Triggered' and 'Reconstructed', respectively. The label '$\cos(\theta) > 0$' corresponds to the events that are (wrongly) reconstructed as upward going. Neutrino events are generated according to a spectrum proportional to $E_\nu^{-1.4}$. By applying different weights to the events (see section 2.10.1), the sample of neutrinos can represent the atmospheric neutrino flux as well as any other assumed signal flux. The standard signal flux is taken to be proportional to E^{-2}.

5.1.1 Angular acceptances

In section 2.6.1, three parameterisations of the angular acceptance of the optical modules were introduced. The differences between these three parameterisations

Rate	60 kHz	120 kHz	240 kHz
Generated	$2.8 \cdot 10^7$	$2.9 \cdot 10^7$	$3.0 \cdot 10^7$
$N_{photons} \geq 10$	4151150	4299453	4447521
Triggered	421813	559537	2095429
Reconstructed	228097	221007	212332
$\cos(\theta) > 0$	11718	13374	16743
Livetime	79735.9 s (0.923 day)	82594.7 s (0.956 day)	85439.2 s (0.989 day)

Table 5.3: *Sample of simulated atmospheric muon events used in this study.*

occur at large angles. This is important when considering the background of atmospheric muons. Consequently, the simulated rate of triggered events due to atmospheric background differs significantly between these parameterisations. One of these parameterisations has been used in the earlier Antares simulation software. This parameterisation was based on measurements of a different optical module design. The more recent parameterisations, which show an increased acceptance at large angles of incidence, were used in the study of the data from Line 1 in chapter 4. In this chapter, the parameterisation from [40] is used. This parameterisation corresponds to our current best knowledge. At 60 kHz background rate, the trigger rate due to atmospheric muons is a factor 2 higher than the rate using the older parameterisation. Previous analyses, for example in reference [74], were done with the old parameterisation and thus predict a lower event rate. The use of a different angular acceptance also has an effect on the rate of events due to upward going (atmospheric) neutrinos. The increase in rate is smaller than that of the atmospheric muons, as the difference between the parameterisations at small angles of incidence is limited to a few percent. Figure 5.1 shows the relative increase in reconstruction rate with the angular acceptance used in this study as function of neutrino energy. It can be seen that the increase is largest at lower energies and decreases towards higher energies. The total increase in rate from atmospheric muons is about 24 %, while for a signal flux proportional to E^{-2} it is 13 %.

5.2 Selections

After track reconstruction, several quantities are available which contain information on the quality and properties of the track. These quantities can be used as selection criteria to suppress the background. Events are selected by requiring a minimum or maximum value for a certain quantity related to the event. This is referred to as applying a cut. The first cut corresponds to the requirement that the event is reconstructed as upward going, thus $\cos(\theta) \geq 0$. In the following several other cuts will be presented.

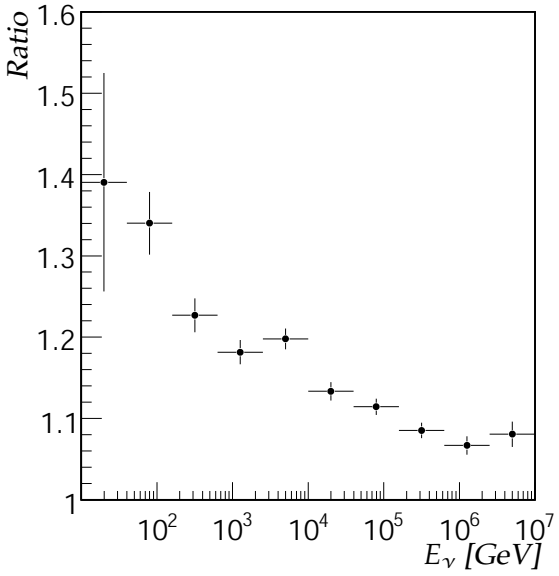

Figure 5.1: *Ratio of the rates of reconstructed neutrinos for different parameterisations of the angular acceptance of the optical modules. The ratio is plotted as function of neutrino energy and given by the rate for the parameterisation given in [40] over the rate for the 'old' (see section 2.6.1) parameterisation. The neutrinos are isotropically generated in upward directions.*

5.2.1 Track length

In section 3.6.7 the track length ($\Delta z'$) was introduced. This quantity is the largest distance between two hits measured along the reconstructed muon track. For this, the hits for the prefit with the smallest angular residual compared to the final likelihood fit are used. Only hits that are included in the selection based on the directional clustering criterion (see section 3.3) are considered. The value $\Delta z'$ can be used as a measure of the accuracy of the muon track reconstruction (see section 3.6.7 and figure 3.29). The distributions of $\Delta z'$ for atmospheric muons, neutrinos and random background events which are reconstructed as upward going are shown in figure 5.2. It can be seen from figure 5.2 that the distribution for atmospheric muons shows an excess of events at small track lengths compared to atmospheric neutrinos and random background events. A prominent feature of the $\Delta z'$ distribution for atmospheric muons is the triple peaked structure. These peaks can clearly be distinguished in figure 5.2 at around 70, 130 and 190 meters. The typical distances between two detector lines vary from about 60 to 70 meters (see figure 2.8). The three peaks correspond to hits on 2, 3 and 4 lines respectively. In the context of the analysis of the data of a single line, it was shown that electro-magnetic showers along a muon track can bias the reconstruction to horizontal directions (see section 4.5). This affects in particular the atmospheric muons due to the orientation of the optical modules. Two peaks can be seen in the distribution of atmospheric neutrinos. These peaks are shifted to higher values of $\Delta z'$ compared to the 3 and 4 line peaks of the atmospheric muons. The shifts are due to the angular distribution of the atmospheric neutrinos, which covers the complete upward going solid angle. The peak at $\Delta z' \simeq 200$ m which can also be seen in the distribution of random background events, corresponds to the typical

	60 kHz	120 kHz	240 kHz
Atmospheric ν	84.4 %	89.4 %	86.8 %
Atmospheric μ	49.9 %	59.7 %	56.8 %
Random background	–	94.0 %	90.5 %

Table 5.4: *Fractions of remaining events after requiring a minimum length of the reconstructed track ($\Delta z^{'}$) of 120 meters for different random background rates.*

length scale of the detector for an isotropic muon flux and a random background.

In order to reject a fraction of the background of wrongly reconstructed atmospheric muons, a cut on $\Delta z^{'}$ is applied. Only upward reconstructed tracks with $\Delta z^{'} > 120$ m are accepted. The remaining fractions of atmospheric muons, atmospheric neutrinos and random background events are given in table 5.4. As can be seen from table 5.4, the cut on $\Delta z^{'}$ is most effective on wrongly reconstructed atmospheric muons. Events due to random background are least affected.

5.2.2 Up/Down likelihood

The muon track reconstruction algorithm scans over 4π solid angle and produces in general a set of different track candidates. In section 3.6.5, the use of the relative values of the log-likelihood per degree of freedom was introduced as a way to select the best track candidate. The track candidate with the largest log-likelihood per degree of freedom is selected. As shown in chapter 3, it is possible that a solution which differs from the true track, has a higher log-likelihood per degree of freedom than the true track. This can happen when the processes that have led to the recorded hits are different from the assumed (muon) hypothesis or due to statistical fluctuations. It is possible to consider the best upward and the best downward reconstructed track separately. For this purpose, the largest value of the likelihood per degree of freedom given by L^{up}/N^{up}_{dof} and L^{down}/N^{down}_{dof} can be used, where the superscript up and down refer to the upward and downward directions. The difference of these values

$$\Delta L = L^{up}/N^{up}_{dof} - L^{down}/N^{down}_{dof} \tag{5.1}$$

can be used to reject background events which are wrongly reconstructed as upward going. In figure 5.3, the fraction of remaining events for a given minimum value of ΔL is shown for neutrinos, atmospheric muons and random background events. The plateau in figure 5.3 at large values of ΔL is due to events which have no downward going solution. Several features can be seen in figure 5.3 when comparing atmospheric muons, neutrinos and background events and considering different background rates. First, a larger fraction of the neutrinos has no downward solution at all compared to atmospheric muons. Whereas, almost 80

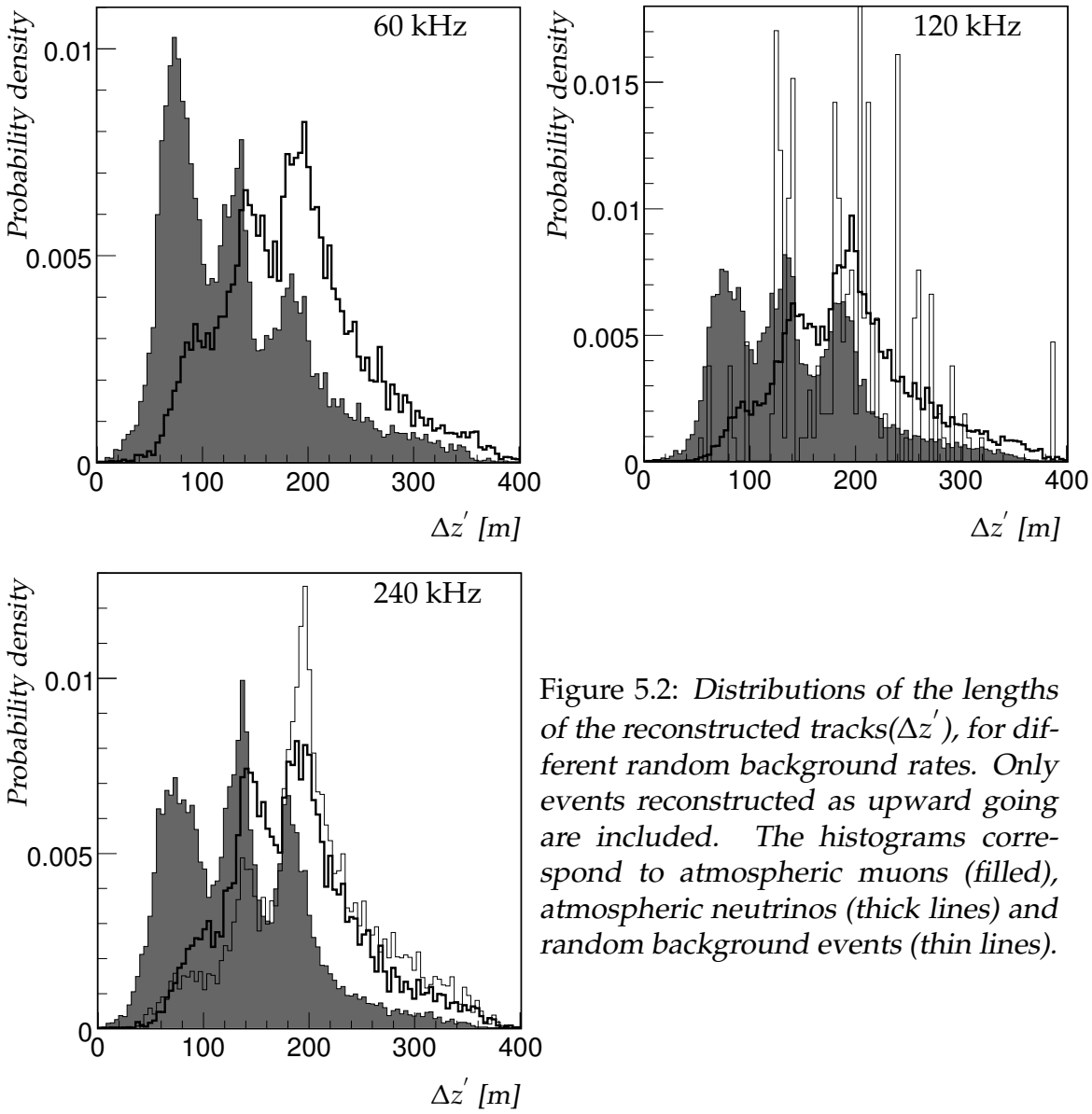

Figure 5.2: *Distributions of the lengths of the reconstructed tracks($\Delta z'$), for different random background rates. Only events reconstructed as upward going are included. The histograms correspond to atmospheric muons (filled), atmospheric neutrinos (thick lines) and random background events (thin lines).*

	60 kHz	120 kHz	240 kHz
Value of cut on ΔL	1.0	0.5	0.3
Remaining atmospheric ν	86.7 %	86.7 %	87.1 %
Remaining atmospheric μ	22.1 %	27.2 %	42.1 %
Remaining random background	– %	93.6 %	89.7 %

Table 5.5: *Values of the cut on ΔL (see text) for different background rates. The numbers correspond to the remaining fractions of events.*

% of the atmospheric muons have a possible downward going solution at 60 kHz, this fraction is 35 % for atmospheric neutrinos. The neutrinos which do have a downward solution have in general a larger value of ΔL compared to the atmospheric muons. This is reflected by the gradient of the distributions at small values of ΔL. The fraction of remaining events drops more steeply for atmospheric muons, than for neutrinos. Thus, a selection on a minimum value of ΔL can reduce the number of upward reconstructed atmospheric muons, whilst retaining a large fraction of the neutrinos. At high rates (120 and 240 kHz) few random background events ($<$ 10%) have a downward solution. Hence, these events show a plateau close to unity. With increasing random background rate, the relative contribution of direct hits from the atmospheric muons is suppressed. At the highest rates, the dead-time of the ARSs comes into play. As a result, the number of atmospheric muon events that are falsely identified as upward going increases. The suppression of muon hits also leads to a lower chance of having a (correct) downward going solution in the set of solutions. This is reflected in the increase of the level of the plateaus at large ΔL for atmospheric muons in figure 5.3 with increasing rate. The effect of increasing background rates is different for the neutrinos, depending on their energy. Increasing the rate from 60 to 120 kHz causes more events to have also a downward going solution. This is due to availability of additional hits. When increasing the rate further to 240 kHz, the contribution of muon hits gets suppressed due to ARS dead-time and random background hits can form a significant fraction of the hits in the events, especially at lower energies. This can even lead to the impossibility of finding enough L1 hits for a given direction in the prefit, and thus rejecting it. The effect on the hit selection can be seen in figure 3.9. So, while the fraction of events with a downward solution increases when increasing the rate from 60 kHz to 120 kHz, it decreases when increasing the rate further to 240 kHz. The crossing of the lines for atmospheric and 'signal' neutrinos in figure 5.3 for 240 kHz reflects that this effect is stronger at lower energies. For each rate, a minimum value for ΔL is determined in such way that the ratio between the fraction of atmospheric neutrinos and the fraction of atmospheric muons is maximal. In table 5.5, the values thus obtained are given, together with the remaining fractions of events.

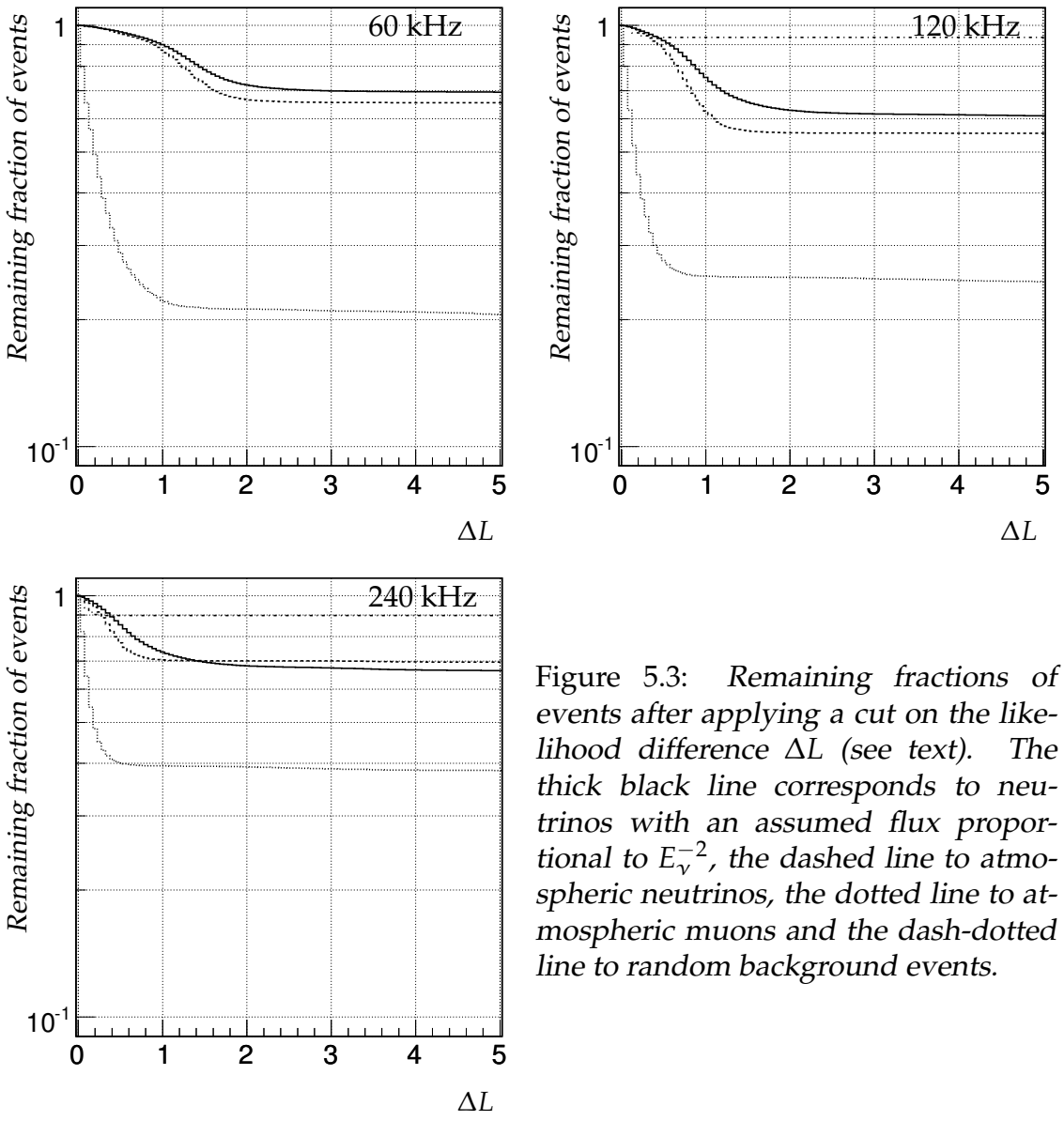

Figure 5.3: *Remaining fractions of events after applying a cut on the likelihood difference ΔL (see text). The thick black line corresponds to neutrinos with an assumed flux proportional to E_ν^{-2}, the dashed line to atmospheric neutrinos, the dotted line to atmospheric muons and the dash-dotted line to random background events.*

5.2.3 Likelihood and number of compatible solutions

The log-likelihood per degree of freedom can be combined with the number of compatible solutions (see section 3.6.8) to obtain a joint quantity, namely :

$$\Lambda = \ln(L)/N_{dof} + 0.1(N_{comp} - 1) \tag{5.2}$$

It was shown in reference [74] that cutting on a minimum value of Λ is very effective in reducing the background of atmospheric muons. The effect of a cut on the value of Λ, including the cuts discussed in the previous two sections, is shown in figure 5.4. In this figure, the remaining number of upward reconstructed events per day due to atmospheric muons, atmospheric neutrinos and random background events is shown as a function of Λ. The efficiencies for a neutrino flux proportional to E^{-2} are also shown. As can be seen from figure 5.4, the background due to atmospheric muons and random noise can be reduced significantly, whilst retaining the neutrino signal(s). For small values of Λ, the wrongly reconstructed atmospheric muons dominate. The contribution from atmospheric neutrinos starts to dominate at $\Lambda \simeq -6$. As was shown in section 3.6.4, an increase of the random background rate, shifts the log-likelihood per degree of freedom to smaller values. The value of N_{comp} also decreases with increasing rate, as shown in section 3.6.8. These two effects result in a shift of Λ to smaller values as can be seen in figure 5.4 for all types of events. The contribution of random background events also increases with increasing background rates, but remains smaller by at least a factor 10 than the contribution from atmospheric muons. As was shown in chapter 3, the angular resolution of reconstructed tracks is correlated with the likelihood per degree of freedom and the number of compatible solutions. The effect of the cut on Λ on the angular resolution is shown in figure 5.5. In this graph, the angular resolution for an atmospheric neutrino spectrum and a neutrino energy spectrum proportional to E^{-2} is shown for different random background rates. Several observations can be made when comparing the different neutrino spectra and considering the different random background rates. The values without a cut on Λ reflect the deterioration of the angular resolution with increasing random background rates (see also figure 3.26). The differences between the results for the two neutrino fluxes, reflect the dependence of the angular resolution on the muon energy (see also figure 3.26). The E^{-2} spectrum is harder than that of the atmospheric neutrinos. As the angular resolution improves with energy, the overall resolution for a E^{-2} spectrum is better. At larger values of the cut on Λ, the relative improvement of the angular resolution depends on the background rates. In short, the improvement of the angular resolution is larger for higher random background rates. Increasing Λ has a more severe effect on the angular resolution of the remaining events at higher background rates. This can be seen in figure 5.5 by the different gradients of the lines. This has to be considered together with the decreasing efficiency as shown in figure 5.4. For each background rate, the value of the cut on Λ is

Rate	cut value on Λ	Atmospheric neutrinos	Signal efficiency
60 kHz	-5.3	9.7/day	66.8 %
120 kHz	-5.5	6.2/day	61.6 %
240 kHz	-5.9	4.9/day	55.9 %

Table 5.6: *Values of the cut on Λ for different random background rates and the corresponding rates of atmospheric neutrinos and efficiencies for a neutrino signal with a flux proportional to E_ν^{-2}.*

chosen such that the remaining events due to atmospheric muons is 1 per day. The background is then dominated by atmospheric neutrinos. In order to reduce the uncertainty on the value of the cut due to the limited statistics, the value is determined from an exponential fit to the distributions. This fit is applied to the differential distributions of the data. The lower bound is chosen such that the uncertainty of the slope from the fit is less than 10 %. The values for the cut on Λ which result from these fits are shown in table 5.6, together with the fractions of remaining events.

5.3 Effective area

The detector efficiency is usually expressed as the neutrino effective area. The neutrino effective area A_ν^{eff} is defined as the ratio of the rate of reconstructed events and the incident neutrino flux :

$$A_\nu^{eff}(E_\nu, \theta, \phi) = \frac{R_{det}(E_\nu, \theta, \phi)}{\Phi_\nu(E_\nu, \theta, \phi)} \tag{5.3}$$

In this equation, R_{det} is the rate of reconstructed events and Φ_ν the neutrino flux arriving at the surface of the Earth. The effective area includes the neutrino cross section, the propagation of neutrinos through the Earth and the detection of the muons. The detection rate is determined by reconstruction and selection criteria defined previously. Thus, the neutrino effective area incorporates the reconstruction efficiency and the inefficiencies introduced by the selection cuts to reduce background. Using this definition, the rate of observed neutrino events can directly be determined for any given neutrino flux. The neutrino effective area depends on the neutrino energy and direction. In figure 5.6, the neutrino effective area is shown for upward directions and different ranges in zenith angle. The strong dependence of the neutrino effective area on the neutrino energy comes mainly from the energy dependence of the cross section (see figure 2.1) and the increase of the range of the muon. The reduction of the neutrino effective area for upward directions at very high energies is caused by the absorption of neutrinos

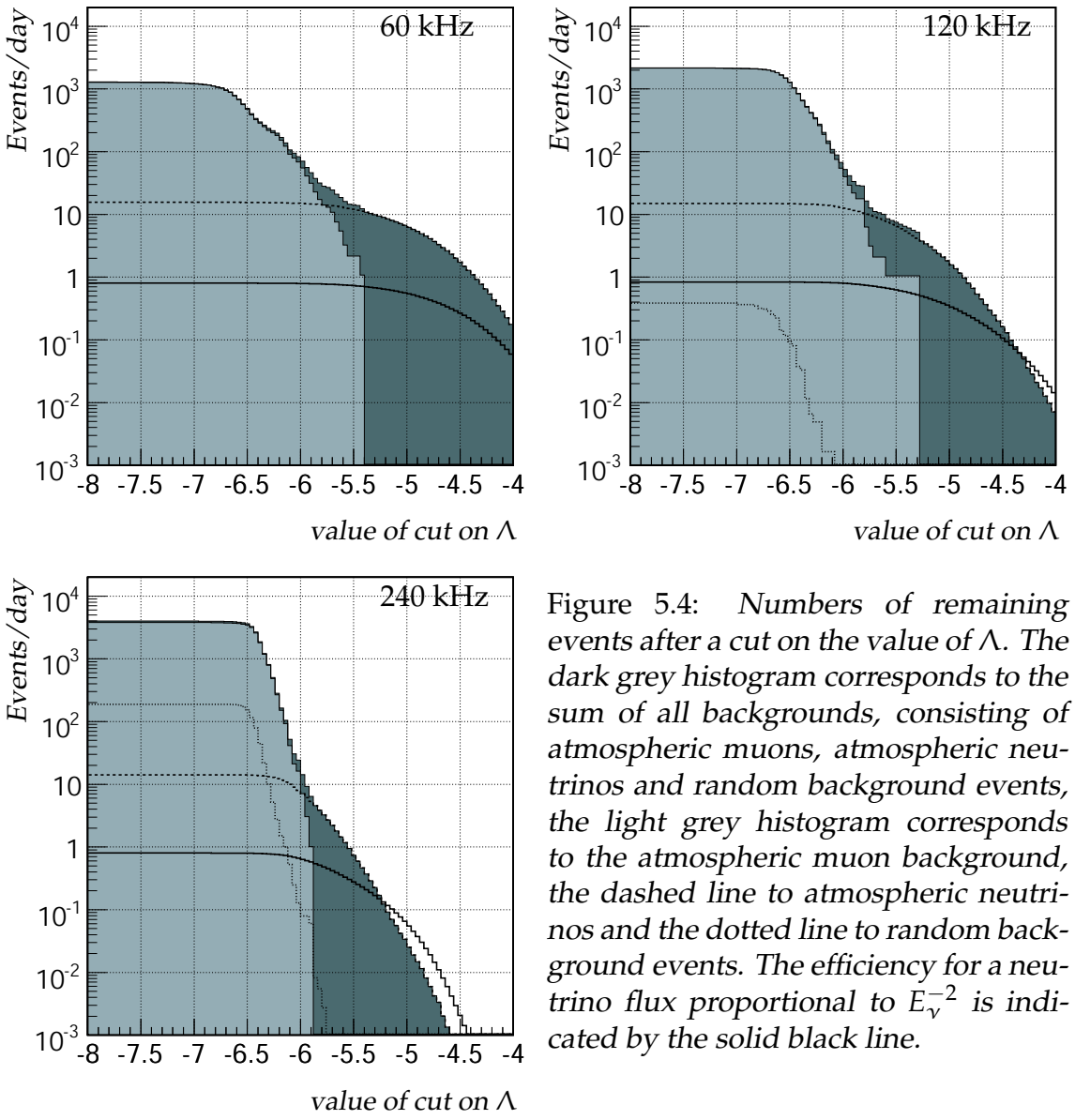

Figure 5.4: *Numbers of remaining events after a cut on the value of Λ. The dark grey histogram corresponds to the sum of all backgrounds, consisting of atmospheric muons, atmospheric neutrinos and random background events, the light grey histogram corresponds to the atmospheric muon background, the dashed line to atmospheric neutrinos and the dotted line to random background events. The efficiency for a neutrino flux proportional to E_ν^{-2} is indicated by the solid black line.*

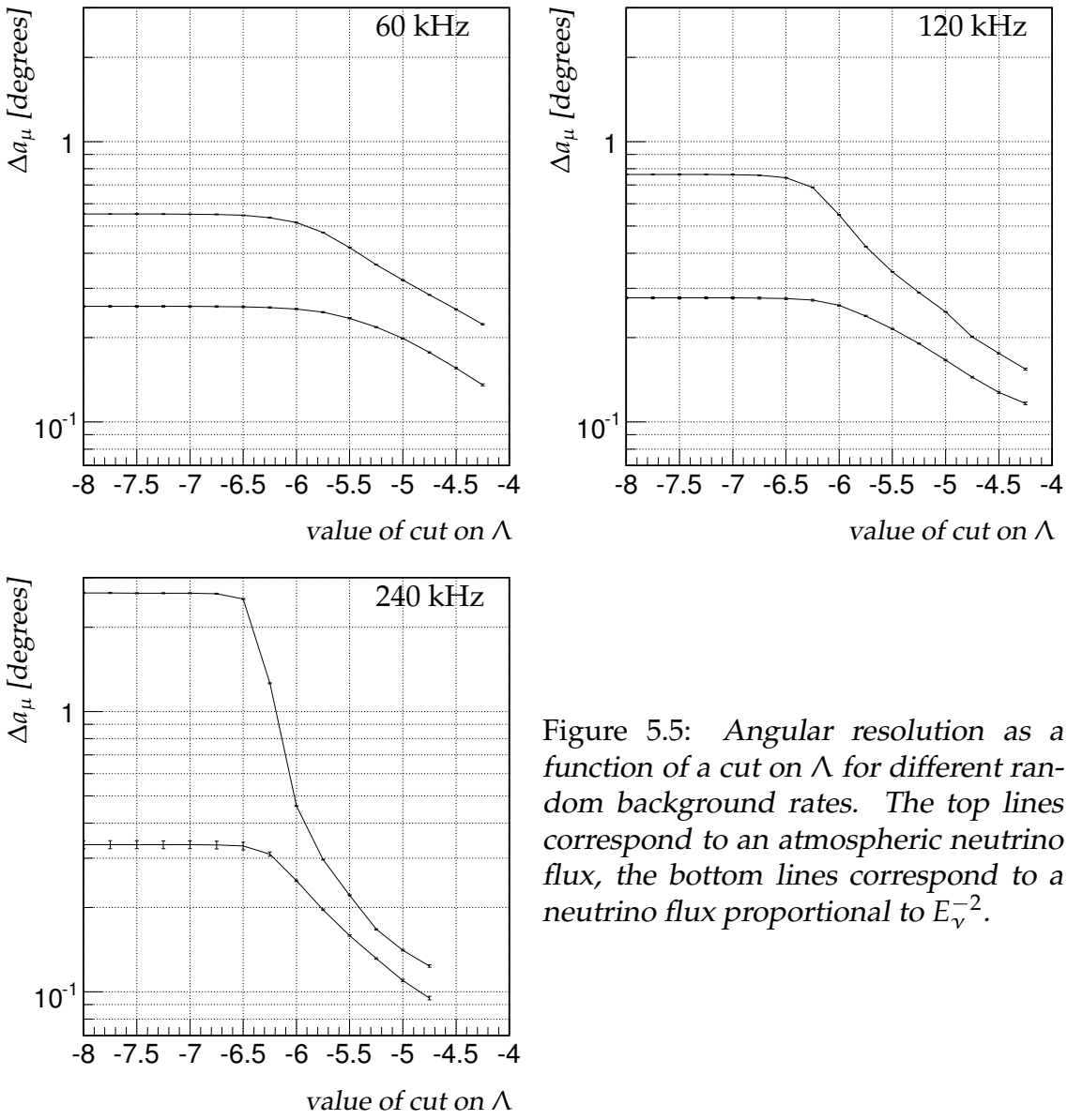

Figure 5.5: *Angular resolution as a function of a cut on Λ for different random background rates. The top lines correspond to an atmospheric neutrino flux, the bottom lines correspond to a neutrino flux proportional to E_ν^{-2}.*

in the Earth. In general, the neutrino effective area reduces with increasing random background rates. This effect is more prominent at lower energies. In figure 5.7, the ratios of the neutrino effective areas are shown as function of the energy integrated over all upward directions. The random background rate mostly affects the neutrino effective area at lower neutrino energies. Compared to the effective area at 60 kHz, the effective areas for 120 and 240 kHz differ up to a factor 2 between about 100 and 300 GeV. With increasing neutrino energy, the effective areas differ less. Compared to 60 kHz, the loss in effective area at 10^7 GeV is less than 5 % at 120 kHz and less than 10 % at 240 kHz.

5.4 Angular resolution

The median of the angular residual distributions is used to quantify the angular resolution of the detector. The resolution for the muon direction is presented in chapter 3. In this chapter, several cuts were introduced which are used to reduce the background. These cuts affect the efficiency of the detector as well as the angular resolution. The angular resolution for muons is shown as a function of the variable Λ in figure 5.5. The relevant quantity for the pointing accuracy of the telescope is the angular residual for neutrinos. The accuracy of the determination of the neutrino direction depends on the energy in two ways. The actual reconstruction is done on the muon, and the angular resolution of the reconstruction depends on the muon energy. In general, the angular resolution of the reconstruction improves with increasing energy due to the increase of the detectable photon yield. The neutrino direction is obtained by assuming the same direction as that of the muon. This introduces an additional error, as the muon and neutrino directions are related through the finite scattering angle. The average scattering angle decreases with the neutrino energy (see section 2.2). The resolutions for the muon and neutrino direction are studied after applying the cuts which were introduced earlier in this chapter. In figure 5.8, the angular resolution for muon and neutrino directions are shown as function of neutrino energy for different random background rates. As can be seen from figure 5.8, the resolution improves with energy. The angular resolution does not depend significantly on the random background rate. It can be seen from figure 5.8 that for neutrino energies in excess of 100 TeV the angular resolution for neutrinos is limited by the accuracy of the reconstruction.

5.5 Comparison

The detector performance using the muon track reconstruction and cuts developed in this work, can be compared to the performance when using the standard reconstruction [74]. The standard reconstruction was developed and evaluated

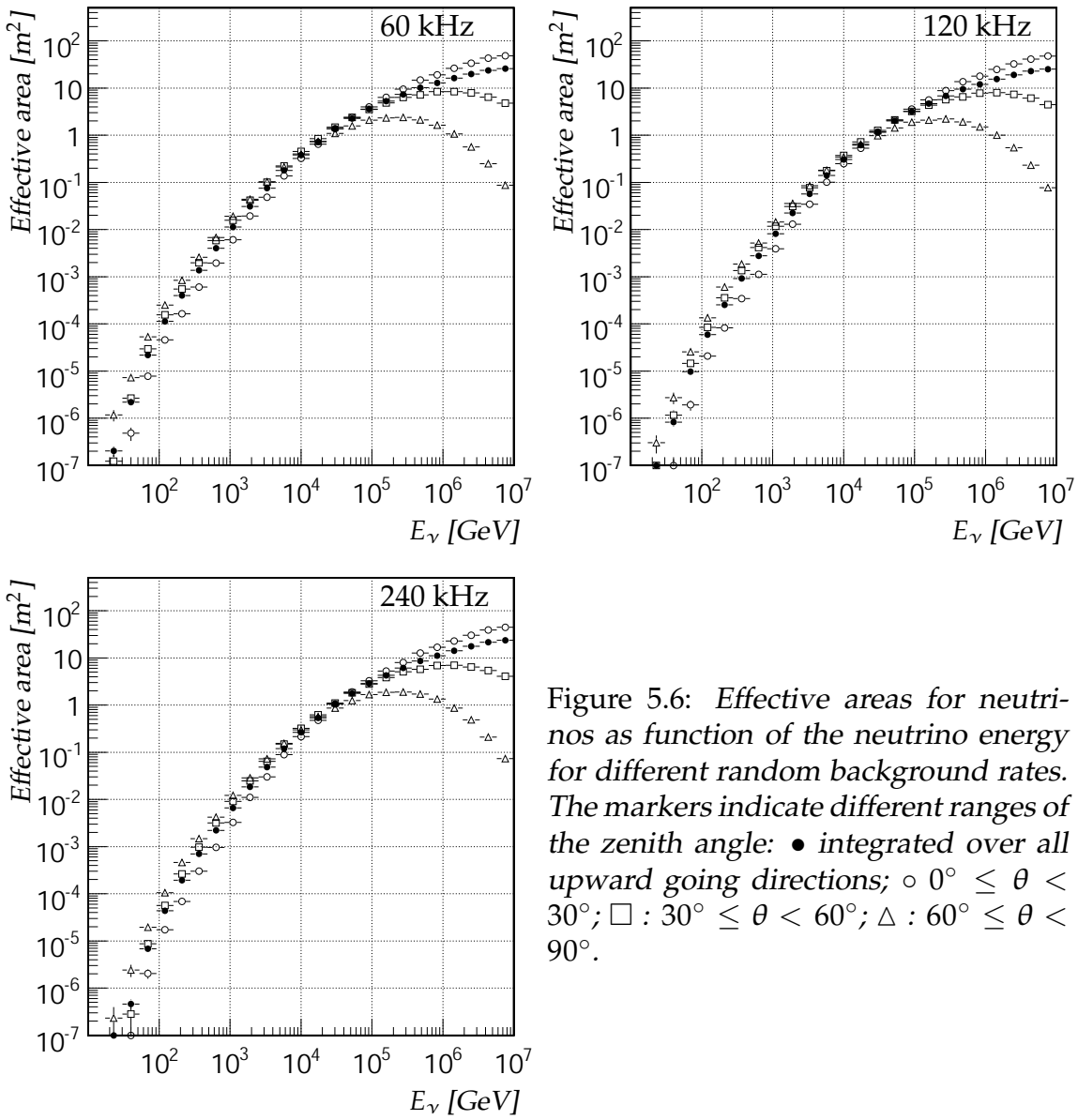

Figure 5.6: *Effective areas for neutrinos as function of the neutrino energy for different random background rates. The markers indicate different ranges of the zenith angle:* • *integrated over all upward going directions;* ∘ $0° \leq \theta < 30°$; □ : $30° \leq \theta < 60°$; △ : $60° \leq \theta < 90°$.

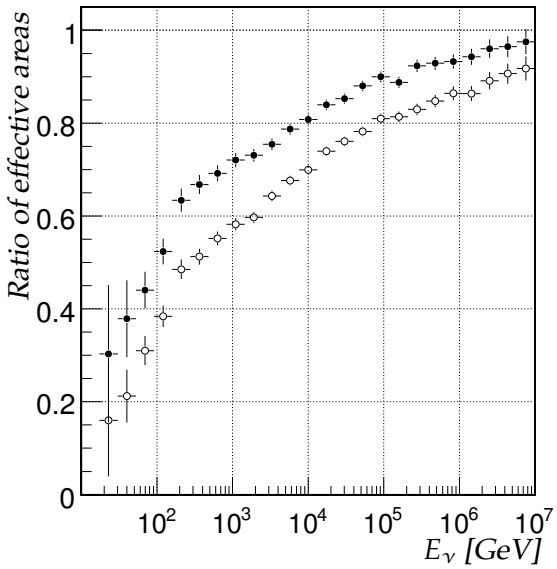

Figure 5.7: *Ratios of effective areas for different background rates as function neutrino energy. The filled dots indicate the ratio of the effective area at 120 kHz over the effective area at 60 kHz. The open dots indicate the ratio of the effective area at 240 kHz over the effective area at 60 kHz.*

under different conditions. These conditions were the absence of the current trigger algorithm and the use of an old parameterisation of the angular acceptance of the optical modules. As shown previously, the use of the current parameterisation leads to an increase in detected photons and event rates compared to the old parameterisation. The comparison is done at a random background rate of 60 kHz. In the standard reconstruction, the final cut to reduce background is similar to the one presented in this work. It is based on the quantity defined in equation 5.2. However, the PDF used in the final stage of the standard reconstruction differs from the one developed in this work. The cut value used in the standard reconstruction is referred to as Λ_s. The value for the cut on Λ_s which reduces the rate of atmospheric muons (neutrinos) to about 1/day (10/day) was previously [74] determined to be -5.3. This cut is re-evaluated, to take into account the new angular acceptance. In figure 5.9, the remaining number of atmospheric muons and neutrinos is shown as function of the value of the cut on Λ_s. Also shown is the efficiency for a signal proportional to E_ν^{-2}. From this figure, it can be seen that when a cut $\Lambda_s > -5.3$ is applied, the remaining rates of atmospheric muons and neutrinos are both about 10/day. In order to reduce the background of atmospheric muons to about 1/day using AartStrategy, the minimal value of Λ_s is set to -5. The rate of atmospheric neutrinos is then about 8/day. With this newly determined cut on the value of Λ_s, the effective area and angular resolution are compared with those presented in this work. In figure 5.10 both effective areas are shown. It can be seen that the effective area is increased at energies below about 4 TeV and above about 50 TeV. At 10 PeV, the increase in effective area reaches about a factor 2. This increase can be attributed to the better description of the PDF at these high energies (see section 3.5). At 100 GeV, the increase is about 40 %. The angular resolutions as function of neutrino energy are compared in figure 5.11. The angular resolutions are almost identical, with the standard

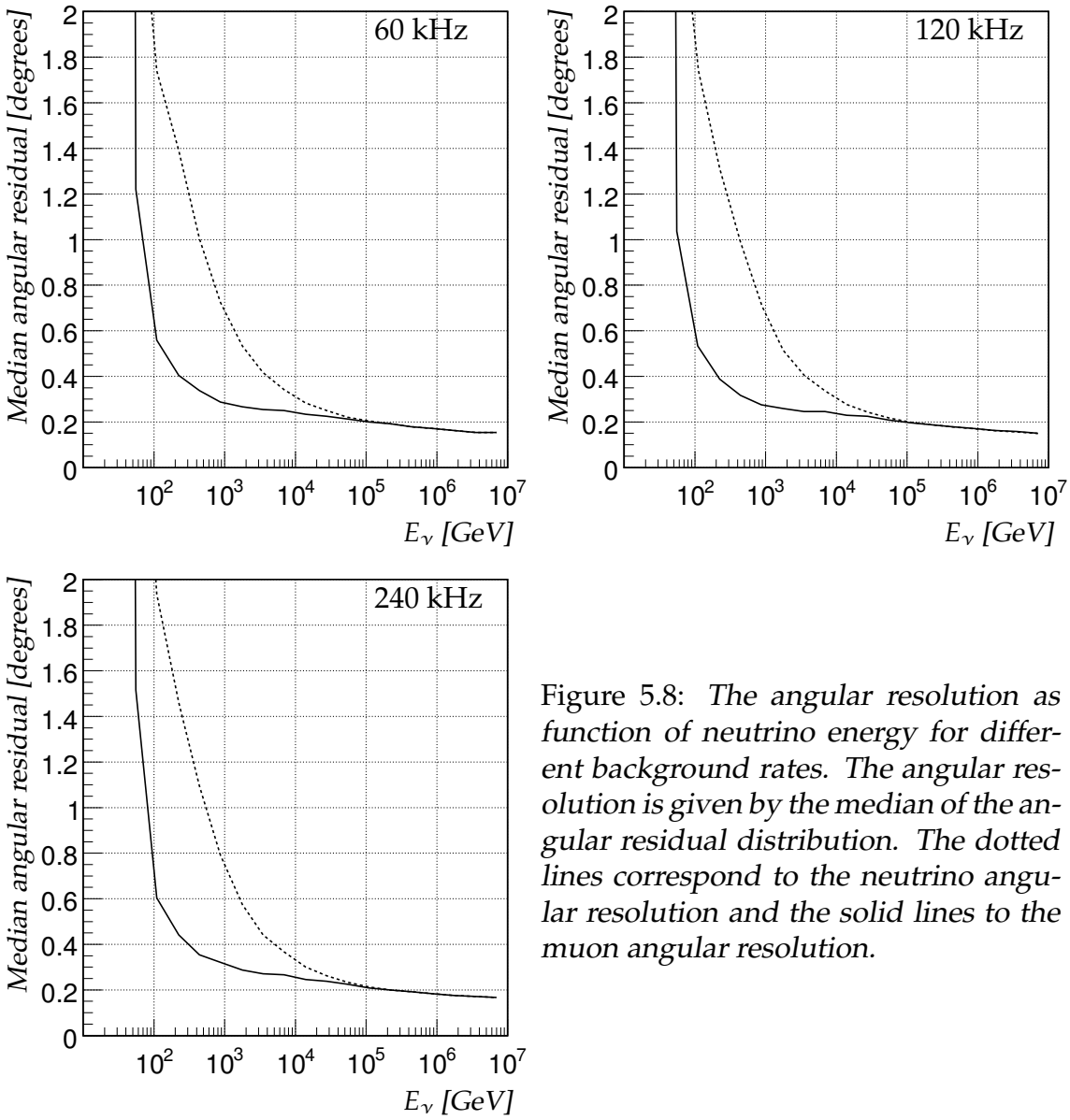

Figure 5.8: *The angular resolution as function of neutrino energy for different background rates. The angular resolution is given by the median of the angular residual distribution. The dotted lines correspond to the neutrino angular resolution and the solid lines to the muon angular resolution.*

reconstruction having a small advantage at lower energies and the new one at higher energies. When considering a neutrino flux proportional to E^{-2}, the median angular residual is about 0.26° for both the old and new methods.

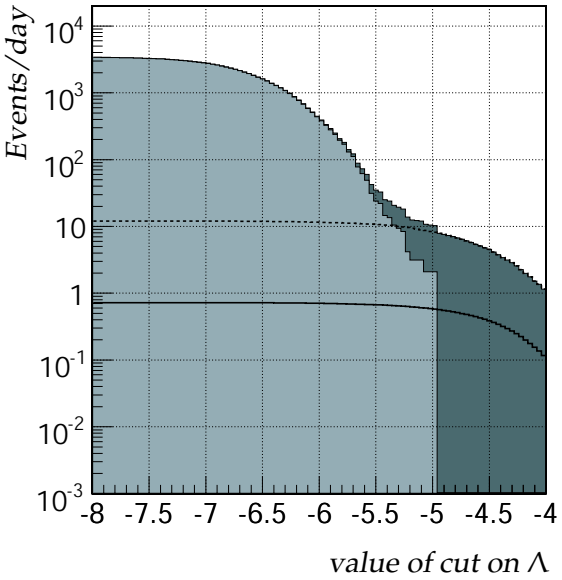

Figure 5.9: *Numbers of remaining events after a cut on the value of Λ, using the muon track reconstruction algorithm from [74]. The random background rate is 60 kHz. The dark grey histogram corresponds to the sum of all backgrounds, consisting of atmospheric muons, atmospheric neutrinos and random background events, the light grey histogram corresponds to the atmospheric muon background, the dashed line to atmospheric neutrinos and the dotted line to random background events. The efficiency for a neutrino flux proportional to E_ν^{-2} is indicated by the solid black line.*

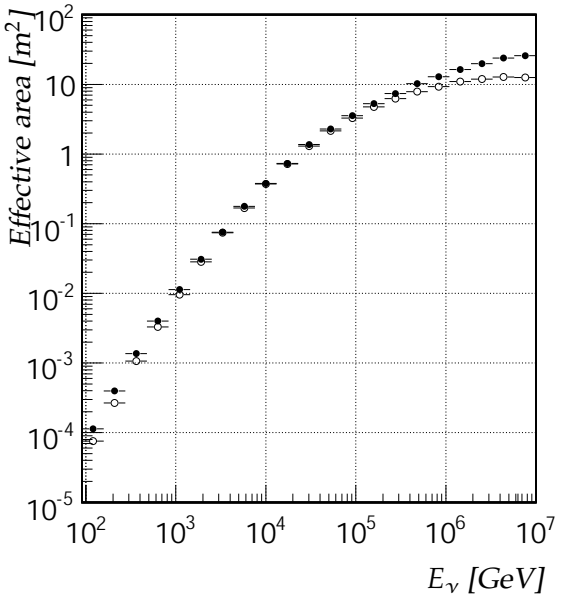

Figure 5.10: *Comparison of effective areas for neutrinos as function of the neutrino energy at a background rate of 60 kHz. The effective areas are integrated over all upward going directions. • : this work; ○ : using the muon track reconstruction algorithm and cuts from [74]*

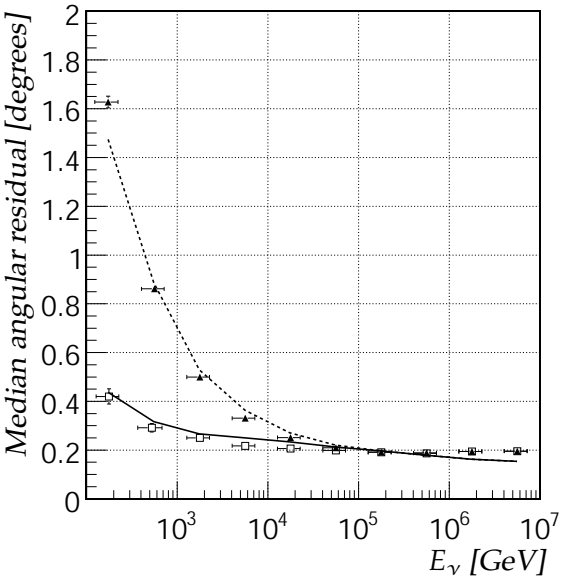

Figure 5.11: *The angular resolution as function of neutrino energy at a background rate of 60 kHz. The angular resolution is given by the median of the angular residual distribution. The lines correspond to the muon track algorithm developed in this work, the points to the algorithm and cuts from reference [74]. The dotted line and filled triangles correspond to the neutrino angular resolution and the solid line and open squares to the muon angular resolution.*

5.6 Conclusion

In this chapter the reconstruction method developed in this work was evaluated in the presence of backgrounds. The trigger algorithm and the new parameterisation of the angular acceptance have been taken into account. Several cuts have been presented that reduce the backgrounds from atmospheric muons and random background rate. The detector performance has been evaluated with these cuts applied. The resulting effective area and angular resolution have been presented. The effective area of the Antares detector depends on the random background rate. When the level of random background increases, the effective area is reduced. The reduction in effective area is stronger at lower neutrino energies. The angular resolution remains at the same level as the standard reconstruction, evaluated at 60 kHz random background rate. The effective area improves upon the previous effective area. Below 4 TeV and above 50 TeV neutrino energy, the effective area is increased up to a factor 2 at 10 PeV neutrino energy.